Eur. Phys. J. C 9, 425–435 (1999)
Digital Object Identifier (DOI) 10.1007/s100529900049

THE EUROPEAN PHYSICAL JOURNAL C

Production of light fermion–antifermion pairs in $\gamma\gamma$ collisions

A. Denner[1], S. Dittmaier[2]

[1] Paul Scherrer Institut, CH-5232 Villigen PSI, Switzerland
[2] Theory Division, CERN, CH-1211 Geneva 23, Switzerland

Received: 18 December 1998 / Revised version: 1 March 1999 / Published online: 18 June 1999

Abstract. The $\mathcal{O}(\alpha)$ corrections to $\gamma\gamma \to f\bar{f}$ in the standard model are calculated for arbitrary light fermions f. The relevant analytical results are listed in a form that is appropriate for practical applications, and numerical results for integrated cross sections are discussed. The corresponding QED corrections are generally of the order of some per mille for arbitrary energies. The weak corrections to $\gamma\gamma \to \mathrm{e}^-\mathrm{e}^+$ are negligible below the electroweak scale, reach the percent level at a few hundred GeV, and grow to about -10% at 2 TeV. The weak corrections to $\mathrm{u}\bar{\mathrm{u}}$ and $\mathrm{d}\bar{\mathrm{d}}$ production have a shape similar to the one for $\mathrm{e}^-\mathrm{e}^+$, but they are larger by factors of about 1.4 and 3, respectively.

1 Introduction

Since the suggestion of a photon linear collider (PLC) in the eighties [1] as an additional option for future $\mathrm{e}^+\mathrm{e}^-$ linear colliders, many studies on the feasibility (see [2] and references therein) and the physics potential [2,3] of such a machine have been performed. A PLC provides an excellent device that is complementary to $\mathrm{e}^+\mathrm{e}^-$ colliders, as can be seen from the following examples. Photon–photon collisions allow for a search of Higgs bosons by s-channel production and for high-precision tests of the properties of W bosons, which are produced in pairs with an enormously large cross section. Moreover, the production cross sections of charged particles in many models of new physics are even larger than for comparable $\mathrm{e}^+\mathrm{e}^-$ machines [3]. Last, but not least, a PLC allows for various QCD studies, in particular the investigation of the structure of the photon itself.

According to the DESY/ECFA study [2], a total $\gamma\gamma$ luminosity of $10^{33}\,\mathrm{cm}^{-2}\,\mathrm{s}^{-1}$, or even 1–2 orders of magnitude higher, can be reached by Compton backscattering of laser photons off the high-energetic $\mathrm{e}^\pm$ beams in a 500 GeV collider. This production mechanism renders the luminosity spectrum nontrivial, since neither photon beam is monochromatic, and a luminosity monitor has to be sensitive to both photon energies. For this task, the processes $\gamma\gamma \to \mathrm{e}^-\mathrm{e}^+, \mu^-\mu^+$ have been suggested (see [2] and references therein) as reference reactions. Thus, the lepton-pair-production cross section should be known to very high precision.

Exploiting crossing symmetry, the cross sections and corrections for $\gamma\gamma \to \mathrm{e}^-\mathrm{e}^+(\gamma)$ can be obtained from the ones for $\mathrm{e}^+\mathrm{e}^- \to \gamma\gamma(\gamma)$ or $\mathrm{e}^-\gamma \to \mathrm{e}^-\gamma(\gamma)$, which have been studied in the literature (see [4–7] and references therein). However, for $\mathrm{e}^+\mathrm{e}^- \to \gamma\gamma$, only results for unpolarized photons have been published, and the formulas for $\gamma\gamma \to f\bar{f}$, $f \neq \mathrm{e}^-$, cannot be obtained from the above reactions. Therefore, we have performed an independent calculation, and have used the existing results only for checking.

In this paper we calculate the complete $\mathcal{O}(\alpha)$ corrections to $\gamma\gamma \to f\bar{f}$ in the standard model (SM) for arbitrary light fermions f. We present analytical results that are sufficient for an evaluation of all relevant observables, e.g., cross sections and distributions for all polarization configurations. The structure of the radiative corrections and the leading contributions are discussed in detail. Moreover, we provide numerical results on the integrated cross sections and the corresponding electroweak corrections for the different fermion flavours.

The paper is organized as follows: In Sect. 2, we introduce some conventions and list analytical results for the lowest-order cross sections. In Sect. 3, the electroweak radiative corrections are classified into QED and weak corrections, and the corresponding analytical results are presented. The numerical results are discussed in Sect. 4, and Sect. 5 contains a summary. Explicit analytical expressions for the relevant scalar one-loop integrals are given in the appendix.

2 Conventions and lowest-order cross sections

We consider the reaction

$$\gamma(k_1,\lambda_1) + \gamma(k_2,\lambda_2) \longrightarrow f(p,\sigma) + \bar{f}(\bar{p},\bar{\sigma}). \qquad (1)$$

The mass m_f of the fermion f is neglected whenever possible. Otherwise we follow closely the conventions of [8]. The helicities of the incoming photons and of the outgoing fermions are denoted by $\lambda_{1,2} = \pm 1$ and $\sigma, \bar{\sigma} = \pm 1/2$,

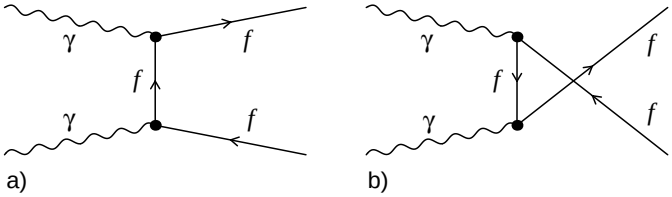

Fig. 1a,b. Tree diagrams for $\gamma\gamma \to f\bar{f}$

respectively. In the center-of-mass system (CMS), the momenta read

$$\begin{aligned} k_1^\mu &= E(1,0,0,-1), \\ k_2^\mu &= E(1,0,0,1), \\ p^\mu &= E(1,-\sin\theta,0,-\cos\theta), \\ \bar{p}^\mu &= E(1,\sin\theta,0,\cos\theta), \end{aligned} \tag{2}$$

where E is the energy of the incident photons, and θ denotes the scattering angle. The Mandelstam variables are given by

$$\begin{aligned} s = (k_1+k_2)^2 &= (p+\bar{p})^2 &&= 4E^2, \\ t = (k_1-p)^2 &= (k_2-\bar{p})^2 &&= -4E^2\sin^2\tfrac{\theta}{2}, \\ u = (k_1-\bar{p})^2 &= (k_2-p)^2 &&= -4E^2\cos^2\tfrac{\theta}{2}. \end{aligned} \tag{3}$$

The neglect of m_f in the kinematics implies that our results are valid for $s, -t, -u \gg m_f^2$.

The scattering amplitude of $\gamma\gamma \to f\bar{f}$ obeys Bose symmetry with respect to the incoming photons and – neglecting quark mixing – CP symmetry also. Consequently, the polarized cross sections $\mathrm{d}\sigma^{\lambda_1,\lambda_2,\sigma,\bar{\sigma}}$ are related by

$$\begin{aligned} &\mathrm{d}\sigma^{\lambda_1,\lambda_2,\sigma,\bar{\sigma}}(s,t,u) \\ &= \mathrm{d}\sigma^{\lambda_2,\lambda_1,\sigma,\bar{\sigma}}(s,u,t) && \text{(Bose)} \\ &= \mathrm{d}\sigma^{-\lambda_1,-\lambda_2,-\bar{\sigma},-\sigma}(s,u,t) && \text{(CP)} \\ &= \mathrm{d}\sigma^{-\lambda_2,-\lambda_1,-\bar{\sigma},-\sigma}(s,t,u) && \text{(Bose + CP)}. \end{aligned} \tag{4}$$

In lowest order, $\gamma\gamma \to f\bar{f}$ is a pure QED process and is therefore invariant under parity (P). Hence, the Born cross sections obey the additional relations

$$\mathrm{d}\sigma_{\mathrm{Born}}^{\lambda_1,\lambda_2,\sigma,\bar{\sigma}}(s,t,u) = \mathrm{d}\sigma_{\mathrm{Born}}^{-\lambda_1,-\lambda_2,-\sigma,-\bar{\sigma}}(s,t,u) \quad \text{(P)}. \tag{5}$$

The two lowest-order Feynman diagrams[1] are shown in Fig. 1. The differential Born cross section reads

$$\begin{aligned} \frac{\mathrm{d}\sigma_{\mathrm{Born}}}{\mathrm{d}\Omega}(P_1,P_2) &= \frac{N_f^{\mathrm{c}}}{64\pi^2 s} \\ &\times \sum_{\lambda_1,\lambda_2,\sigma,\bar{\sigma}} \frac{1}{4}(1+\lambda_1 P_1)(1+\lambda_2 P_2)|\mathcal{M}_{\mathrm{Born}}^{\lambda_1,\lambda_2,\sigma,\bar{\sigma}}(s,t,u)|^2, \end{aligned} \tag{6}$$

where $P_{1,2}$ are the degrees of beam polarization, and the sum on the right-hand side (r.h.s.) includes the desired polarizations of the outgoing particles. The colour factor for the fermion f is denoted by N_f^{c}, i.e., $N_{\mathrm{lepton}}^{\mathrm{c}} = 1$ and $N_{\mathrm{quark}}^{\mathrm{c}} = 3$. The squares of the helicity amplitudes $\mathcal{M}_{\mathrm{Born}}^{\lambda_1,\lambda_2,\sigma,\bar{\sigma}}$ are given by

$$|\mathcal{M}_{\mathrm{Born}}^{\lambda_1,\lambda_2,\sigma,\bar{\sigma}}(s,t,u)|^2 = \begin{cases} 4Q_f^4 e^4 \dfrac{u}{t} & \text{for } \lambda_1 = -\lambda_2 = \pm 1, \\ & \sigma = -\bar{\sigma} = \pm\frac{1}{2}, \\ 4Q_f^4 e^4 \dfrac{t}{u} & \text{for } \lambda_1 = -\lambda_2 = \mp 1, \\ & \sigma = -\bar{\sigma} = \pm\frac{1}{2}, \\ 0 & \text{otherwise.} \end{cases} \tag{7}$$

The t- and u-channel poles in the squared amplitudes lead to kinematical singularities in the extreme forward and backward directions, where we are not interested in the cross sections, since the fermions escape into the beam pipe. For leptons, these singularities are of course regulated by a finite lepton mass. For light-quark production in the forward and backward directions, purely perturbative calculations are not reliable, since the splitting of a photon into a nearly collinear quark–antiquark pair involves QCD effects at very low scales. We avoid the forward and backward regions by imposing the angular cut

$$\theta_{\mathrm{cut}} < \theta < 180^\circ - \theta_{\mathrm{cut}}. \tag{8}$$

For later convenience, we introduce the step function

$$g_{\mathrm{cut}}(\theta) = \Theta(\theta - \theta_{\mathrm{cut}})\Theta(180^\circ - \theta_{\mathrm{cut}} - \theta), \tag{9}$$

where $\Theta(x)$ is the usual Heaviside distribution. Integrating over a symmetric angular range (8), the contributions of all nonvanishing Born cross sections are equal, and the integrated, unpolarized cross section reads

$$\sigma_{\mathrm{Born}}^{\mathrm{unpol}} = N_f^{\mathrm{c}} Q_f^4 \alpha^2 \frac{4\pi}{s}\left[\ln\left(\frac{1+\cos\theta_{\mathrm{cut}}}{1-\cos\theta_{\mathrm{cut}}}\right) - \cos\theta_{\mathrm{cut}}\right], \tag{10}$$

where $\alpha = e^2/(4\pi)$ is the fine-structure constant.

3 Electroweak radiative corrections

3.1 Classification of $\mathcal{O}(\alpha)$ corrections and general remarks

Since $\gamma\gamma \to f\bar{f}$ is a pure QED process in lowest order, the SM electroweak corrections of $\mathcal{O}(\alpha)$ consist of two separately gauge-invariant types: pure QED corrections and genuinely weak corrections. The QED corrections include real-photon emission (see Fig. 2), virtual-photon exchange (see Fig. 3), and the corresponding counterterms. The weak corrections comprise all one-loop diagrams (and contributions to counterterms) that involve the massive weak gauge bosons W and Z. For vanishing fermion mass m_f, there are no contributions involving Higgs-boson exchange or closed fermion loops[2]. As a consequence, the

[1] All Feynman diagrams in this work have been drawn with the help of FeynArts [9].

[2] There are actually Feynman diagrams involving fermion-loop contributions to the AAZ^*, $AA\chi^*$, and AAH^* vertices. However, these contributions are proportional to the mass of the produced fermion f [8] and are thus neglected.

$\mathcal{O}(\alpha)$ corrections do not depend on the Higgs-boson or top-quark masses, nor on the running of α. The weak corrections can be further classified into two subsets[3]. The first of these subsets includes all diagrams that contain internal Z-boson lines (see Fig. 3), and the corresponding corrections are called *neutral-current* (NC) corrections in this paper. The second subset includes all diagrams with W-boson exchange (see Fig. 4), leading to *charged-current* (CC) corrections. Note that only the CC corrections involve nonabelian couplings among the gauge bosons.

The perturbative QCD corrections can be obtained from the QED corrections by substituting the electromagnetic coupling factor $Q_f^2\alpha$ by the strong coupling factor $4\alpha_s/3$. The definition of a proper two-jet cross section is, however, problematic, because jets of radiated gluons cannot be distinguished from those of quarks. Consequently, a two-jet cross section includes the case where a gluon together with one of the quarks cause the two jets, and one of the quarks disappears in the beam pipe. This contribution is divergent, owing to the t- or u-channel poles that are not cut out by this definition of two-jet events. Therefore, a consistent definition of two-jet events in $\gamma\gamma$ collisions necessarily involves nonperturbative effects, which will not be discussed in this paper.

The renormalization of the $\mathcal{O}(\alpha)$ corrections turns out to be extremely simple for $\gamma\gamma \to f\bar{f}$. For $m_f = 0$, the mass renormalization drops out, and only the wave-function renormalization of the external fields and the charge renormalization are relevant. Note that the photonic wave-function renormalization constant exactly cancels against a corresponding part in the charge renormalization (see for instance [10]), so that no effects from the photonic vacuum polarization remain. Consequently, there is no running in the electromagnetic coupling α for $\gamma\gamma \to f\bar{f}$ in this order. The remaining part of the charge renormalization is the contribution of the photon–Z-boson-mixing self-energy at zero-momentum transfer, which in the usual 't Hooft–Feynman gauge consists of a W-boson loop only and is thus part of the CC corrections.

Virtual one-loop corrections are included in predictions by replacing the squared Born amplitude $|\mathcal{M}_{\text{Born}}|^2$ by $|\mathcal{M}_{\text{Born}}|^2 + 2\,\text{Re}\{\mathcal{M}_{\text{1-loop}}\mathcal{M}^*_{\text{Born}}\}$, where $\mathcal{M}_{\text{1-loop}}$ is the contribution of the one-loop diagrams to the scattering amplitude. Thus, the one-loop correction to a lowest-order cross section is zero whenever the lowest order vanishes, and we can factorize the one-loop correction $\mathrm{d}\sigma_{\text{1-loop}}$ to the differential cross section into the lowest-order cross section $\mathrm{d}\sigma_{\text{Born}}$ and the relative correction $\delta_{\text{1-loop}}$ for each polarization configuration:

$$\mathrm{d}\sigma_{\text{1-loop}} = \delta_{\text{1-loop}}\mathrm{d}\sigma_{\text{Born}}, \qquad \delta_{\text{1-loop}} = \delta_{\text{NC}} + \delta_{\text{CC}} + \delta^{\text{virt}}_{\text{QED}}. \tag{11}$$

According to the above decomposition, $\delta_{\text{1-loop}}$ is split into NC, CC, and QED contributions. Since the Born amplitudes are nonvanishing only for $\lambda_1 = -\lambda_2$ and $\sigma = -\bar{\sigma}$ [see (7)], we introduce $\rho = \text{sgn}(\lambda_1) = -\text{sgn}(\lambda_2)$ and $\kappa = \text{sgn}(\sigma) = -\text{sgn}(\bar{\sigma})$, and indicate the polarization configurations for the relative corrections $\delta_{\dots}$ in (11) by $\delta^{\rho,\kappa}_{\dots}$.

[3] In the R_ξ gauges, these subsets are gauge-independent.

The calculation of the one-loop diagrams has been performed by applying the standard techniques summarized in [10]. More precisely, tensor one-loop integrals are algebraically reduced to scalar integrals, as described in [11], and scalar integrals are computed using the methods and results of [12]. Technically, the algebraic evaluation of the Feynman amplitudes, which have been generated with FeynArts [9], has been carried out in the same way as described in [8] for $\gamma\gamma \to t\bar{t}$. In particular, the algebraic manipulations have been performed again twice, once using FeynCalc [13], and once using our own Mathematica [14] routines. For $\gamma\gamma \to e^-e^+$, the virtual corrections are related to the ones of $e^-\gamma \to e^-\gamma$ [7] by crossing symmetry, which has been used as an additional check for this channel.

The evaluation of the real-photon bremsstrahlung will be described in detail below.

3.2 Weak corrections

The NC corrections for the different polarization channels are related by Bose and parity transformations as follows:

$$\delta^{\rho,\kappa}_{\text{NC}} = \delta^{-\rho,\kappa}_{\text{NC}}\Big|_{t\leftrightarrow u} = \delta^{-\rho,-\kappa}_{\text{NC}} \left(g^{\kappa}_{ff\text{Z}}/g^{-\kappa}_{ff\text{Z}}\right)^2, \tag{12}$$

where $g^{\kappa}_{ff\text{Z}}$ is the generic $\text{Z}f\bar{f}$ coupling,

$$g^{\kappa}_{ff\text{Z}} = -\frac{s_\text{w}}{c_\text{w}}Q_f + \frac{I^3_f}{s_\text{w}c_\text{w}}\delta_{\kappa-}, \tag{13}$$

with $I^3_f = \pm\frac{1}{2}$ denoting the weak isospin of the left-handed component of the fermion f. The cosine c_w of the weak mixing angle is fixed by the ratio of the masses M_W and M_Z of the weak gauge bosons, i.e., $c^2_\text{w} = 1 - s^2_\text{w} = M^2_\text{W}/M^2_\text{Z}$. According to (12), all NC correction factors can be deduced from

$$\begin{aligned}
\delta^{+,-}_{\text{NC}} = \frac{\alpha}{\pi}\left(g^{-}_{ff\text{Z}}\right)^2 \Bigg\{ & \left(1 - \frac{M^2_\text{Z}}{u}\right)\left(\frac{3}{2} + \frac{u}{t} + \frac{M^2_\text{Z}}{2u} - \frac{M^2_\text{Z}}{t}\right) \\
& \times \ln\left(1 - \frac{u}{M^2_\text{Z}}\right) - \frac{u}{t}\ln\left(\frac{s}{M^2_\text{Z}}\right) \\
& + \frac{(s+M^2_\text{Z})^2}{t^2}\left[\ln\left(\frac{s}{M^2_\text{Z}}\right)\ln\left(\frac{M^2_\text{Z}+s}{M^2_\text{Z}-u}\right)\right. \\
& \left. + \text{Li}_2\left(-\frac{s}{M^2_\text{Z}}\right) - \text{Li}_2\left(\frac{u}{M^2_\text{Z}}\right)\right] \\
& - \frac{(t-M^2_\text{Z})^2}{t^2}\left[\ln\left(\frac{s}{M^2_\text{Z}}\right)\ln\left(1 - \frac{t}{M^2_\text{Z}}\right)\right. \\
& \left. + \text{Li}_2\left(\frac{t}{M^2_\text{Z}}\right)\right] + \frac{M^2_\text{Z}}{t} - \frac{M^2_\text{Z}}{2u} - \frac{5}{4}\Bigg\}.
\end{aligned} \tag{14}$$

Note that the contributions to the one-loop correction $\delta_{\text{1-loop}}$ (11) are real quantities; the imaginary parts of the one-loop integrals do not contribute. The NC correction (14) agrees with the corresponding correction in [7] after appropriate crossing. Moreover, we have evaluated the

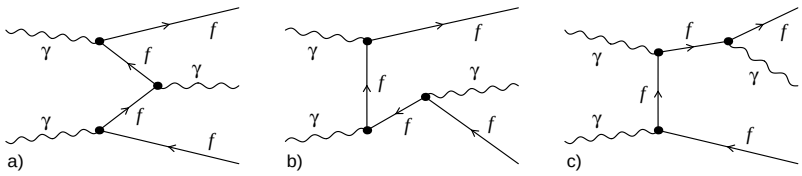

+ crossed graphs

Fig. 2a–c. Diagrams for photon bremsstrahlung in $\gamma\gamma \to f\bar{f}$ ("crossing" means interchanging the incoming photon lines)

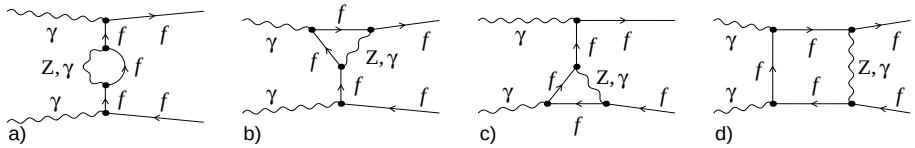

+ crossed graphs

Fig. 3a–d. Diagrams for $\gamma\gamma \to f\bar{f}$ with virtual Z-boson or photon exchange

formulas in [6] for the unpolarized case and find perfect numerical agreement. We could also reproduce the numerical results for the NC corrections in [6].

The CC corrections vanish for right-handed fermions, and the corrections for left-handed fermions are related by Bose symmetry:

$$\delta_{\mathrm{CC}}^{\rho,+} = 0, \qquad \delta_{\mathrm{CC}}^{+,-} = \delta_{\mathrm{CC}}^{-,-}\Big|_{t\leftrightarrow u}. \tag{15}$$

For $\delta_{\mathrm{CC}}^{-,-}$ we explicitly obtain

$$\begin{aligned}
\delta_{\mathrm{CC}}^{-,-} = {} & \frac{\alpha}{4\pi s_{\mathrm{w}}^2}\,\mathrm{Re}\Bigg\{\frac{1}{2} - \frac{3tu + M_{\mathrm{W}}^2 u - 2M_{\mathrm{W}}^2 t}{ut} B_{\mathrm{w}}(t) \\
& + \frac{(Q_{f'} - Q_f)}{Q_f}\,\frac{2(M_{\mathrm{W}}^2 - u)^2}{u^2}\left[t\bar{C}_{\mathrm{ww}}(t) + u\bar{C}_{\mathrm{ww}}(u)\right] \\
& + \frac{(Q_f - Q_{f'})^2}{Q_f^2}\Bigg(\frac{2t}{u}\left[B_{\mathrm{w}}(t) - B_{\mathrm{ww}}(s)\right] \\
& + \frac{st(t+2M_{\mathrm{W}}^2)(t-u)}{u^2} D_{\mathrm{www}}(s,t) \\
& + \frac{t(u-t-2M_{\mathrm{W}}^2)}{u^2}\left[-sM_{\mathrm{W}}^2 D_{\mathrm{www}}(s,t)\right. \\
& \left. + sC_{\mathrm{www}}(s) + 2t\bar{C}_{\mathrm{ww}}(t) + sC_{\mathrm{ww}}(s)\right] \\
& + \frac{(M_{\mathrm{W}}^2 - u)^2}{u^2}\left[(sM_{\mathrm{W}}^2 - st - 2t^2) D_{\mathrm{www}}(s,t)\right. \\
& \left. + (sM_{\mathrm{W}}^2 - su - 2u^2) D_{\mathrm{www}}(s,u) - 2sC_{\mathrm{www}}(s)\right]\Bigg) \\
& + \frac{Q_{f'}(Q_{f'} - Q_f)}{Q_f^2}\,\frac{2(M_{\mathrm{W}}^2 - u)^2}{u^2} \\
& \times \left[(tu + sM_{\mathrm{W}}^2) D_{\mathrm{ww}}(u,t) - t\bar{C}_{\mathrm{w}}(t) - u\bar{C}_{\mathrm{w}}(u)\right] \\
& + \frac{Q_{f'}^2}{Q_f^2}\Bigg(\frac{2t}{u}\left[B(s) - B_{\mathrm{w}}(t)\right] \\
& - \frac{st(2M_{\mathrm{W}}^2 - t - 2u)}{u^2} C_{\mathrm{w}}(s) \\
& + \frac{(s + M_{\mathrm{W}}^2)^2}{u^2}\left[s(M_{\mathrm{W}}^2 - t) D_{\mathrm{w}}(s,t)\right. \\
& \left. + sC(s) + 2t\bar{C}_{\mathrm{w}}(t)\right] \\
& + \frac{(M_{\mathrm{W}}^2 - u)^2}{u^2}\left[s(M_{\mathrm{W}}^2 - u) D_{\mathrm{w}}(s,u) + sC(s)\right. \\
& \left.\left. + 2u\bar{C}_{\mathrm{w}}(u)\right]\Bigg)\Bigg\},
\end{aligned} \tag{16}$$

where $Q_{f'} = Q_f - 2I_f^3$ denotes the charge of the weak isospin partner f' of the fermion f. The functions $B_{\dots}$, $C_{\dots}$, and $D_{\dots}$ are scalar one-loop integrals, the explicit expressions of which are collected in the appendix. Although some of the scalar integrals contain (logarithmic) mass singularities, which are regularized by infinitesimal masses m_f and $m_{f'}$, all mass singularities drop out in the final results for δ_{CC}. For $f = \mathrm{e}^-$, i.e., $Q_{f'} = 0$, (16) is consistent with the corresponding correction to the crossed reaction $\mathrm{e}^-\gamma \to \mathrm{e}^-\gamma$ given in [7]. Although our numerical results on the CC corrections agree quite well with the ones of [6] for the reaction $\mathrm{e}^+\mathrm{e}^- \to \gamma\gamma$ with unpolarized particles, we cannot reproduce the numbers by making use of the formulas given there.

Note that the relative weak corrections vanish directly on the t- and u-channel poles of the lowest-order cross sections, i.e., the weak corrections are suppressed where the differential cross section is maximal. This is a consequence of the usual charge renormalization, which defines the charge $e = \sqrt{4\pi\alpha}$ as the $\gamma f\bar{f}$ coupling for all particles on shell. Since this kinematic situation holds for forward and backward scattering, and since the weak box diagrams do not develop t- and u-channel poles, all weak corrections are absorbed by the corresponding renormalization terms in this special situation.

3.3 QED corrections

3.3.1 Virtual corrections

Bose and P symmetry relate the virtual QED corrections by

$$\delta_{\mathrm{QED}}^{\mathrm{virt},\rho,\kappa} = \delta_{\mathrm{QED}}^{\mathrm{virt},-\rho,\kappa}\Big|_{t\leftrightarrow u} = \delta_{\mathrm{QED}}^{\mathrm{virt},-\rho,-\kappa}, \tag{17}$$

so that it is sufficient to give one particular polarization configuration. Introducing an infinitesimal photon mass

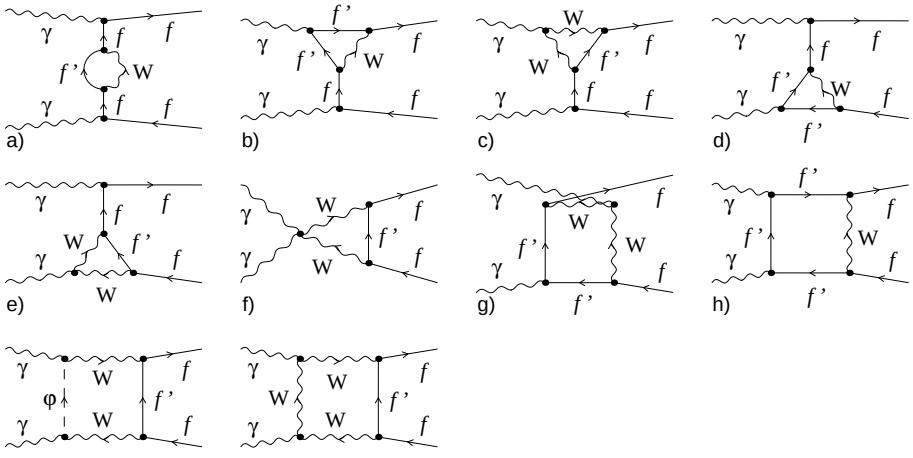

Fig. 4a–j. Diagrams for $\gamma\gamma \to f\bar{f}$ with virtual W-boson exchange

$\lambda \ll m_f$ as infrared (IR) regulator, and keeping m_f in the mass-singular terms, we obtain

$$\begin{aligned}\delta_{\mathrm{QED}}^{\mathrm{virt},+,-} = Q_f^2 \frac{\alpha}{\pi} \Bigg\{ & \ln\left(\frac{-t}{\lambda^2}\right)\left[1+\ln\left(\frac{m_f^2}{s}\right)\right] \\ & -\frac{1}{2}\ln\left(\frac{m_f^2}{-u}\right)+\frac{1}{2}\ln^2\left(\frac{m_f^2}{-t}\right) \\ & +\ln\left(-\frac{s}{t}\right)+\frac{s}{t}\ln\left(-\frac{s}{u}\right)+\frac{s^2}{2t^2}\ln^2\left(-\frac{s}{u}\right) \\ & -\frac{3}{2}+\frac{2\pi^2}{3}\Bigg\}. \end{aligned} \tag{18}$$

Equation (18) can be obtained via crossing from [7]. For the unpolarized case it is consistent with [4,6].

The IR divergence drops out after adding the real-photon bremsstrahlung corrections, and the mass singularities cancel completely against mass-singular real corrections caused by collinear photon emission, since only final-state particles radiate off photons.

3.3.2 Real corrections

Real-photon emission in $\gamma\gamma \to f\bar{f}$ leads to the kinematically different process

$$\gamma(k_1,\lambda_1)+\gamma(k_2,\lambda_2) \;\longrightarrow\; f(p,\sigma)+\bar{f}(\bar{p},\bar{\sigma})+\gamma(k',\lambda'), \tag{19}$$

with k' and λ' denoting the momentum and helicity of the radiated photon, respectively. While the incoming momenta $k_{1,2}$ are the same as for $\gamma\gamma \to f\bar{f}$, as specified in (2), in the CMS, the outgoing momenta read

$$\begin{aligned} p^\mu &= E_f(1,-\cos\phi_f\sin\theta_f,-\sin\phi_f\sin\theta_f,-\cos\theta_f), \\ \bar{p}^\mu &= E_{\bar{f}}(1,\cos\phi_{\bar{f}}\sin\theta_{\bar{f}},\sin\phi_{\bar{f}}\sin\theta_{\bar{f}},\cos\theta_{\bar{f}}), \\ k'^\mu &= E'(1,\cos\phi'\sin\theta',\sin\phi'\sin\theta',\cos\theta'). \end{aligned} \tag{20}$$

The lowest-order cross section for $\gamma\gamma \to f\bar{f}\gamma$, which yields an $\mathcal{O}(\alpha)$ correction to $\gamma\gamma \to f\bar{f}$, is given by

$$\sigma_\gamma(P_1,P_2) = \frac{N_f^{\mathrm{c}}}{2s}\int \mathrm{d}\Gamma \times \sum_{\lambda_1,\lambda_2,\sigma,\bar{\sigma},\lambda'} \frac{1}{4}(1+\lambda_1 P_1)(1+\lambda_2 P_2)\,|\mathcal{M}_\gamma^{\lambda_1,\lambda_2,\sigma,\bar{\sigma},\lambda'}|^2, \tag{21}$$

where the phase-space integral is defined by

$$\int \mathrm{d}\Gamma = \int \frac{\mathrm{d}^3\mathbf{p}}{(2\pi)^3 2E_f}\int \frac{\mathrm{d}^3\bar{\mathbf{p}}}{(2\pi)^3 2E_{\bar{f}}}\int \frac{\mathrm{d}^3\mathbf{k}'}{(2\pi)^3 2E'} \times (2\pi)^4\delta(k_1+k_2-p-\bar{p}-k). \tag{22}$$

We have calculated the helicity amplitudes $\mathcal{M}_\gamma$ in two different ways. One calculation is performed by applying the Weyl–van der Waerden spinor technique (see [15] and references therein); the second calculation makes use of an explicit representation of spinors, polarization vectors, and Dirac matrices. For $m_f = 0$ the helicity structure forces many helicity amplitudes to vanish. In particular, $\mathcal{M}_\gamma$ is zero if $\sigma = \bar{\sigma}$ or $\lambda_1 = \lambda_2 = -\lambda'$. Moreover, Bose, CP, P, and crossing symmetries for in- and outgoing photons lead to relations among the helicity amplitudes. In order to keep things independent of phase conventions, we formulate these relations for $|\mathcal{M}_\gamma|^2$:

$$\begin{aligned} |\mathcal{M}_\gamma^{\lambda_1,\lambda_2,\sigma,\bar{\sigma},\lambda'}|^2 &= |\mathcal{M}_\gamma^{\lambda_2,\lambda_1,\sigma,\bar{\sigma},\lambda'}|^2\Big|_{k_1\leftrightarrow k_2} && \text{(Bose)} \\ &= |\mathcal{M}_\gamma^{-\lambda_1,-\lambda_2,-\bar{\sigma},-\sigma,-\lambda'}|^2\Big|_{p\leftrightarrow\bar{p}} && \text{(CP)} \\ &= |\mathcal{M}_\gamma^{-\lambda_1,-\lambda_2,-\sigma,-\bar{\sigma},-\lambda'}|^2 && \text{(P)} \\ &= |\mathcal{M}_\gamma^{-\lambda',\lambda_2,\sigma,\bar{\sigma},-\lambda_1}|^2\Big|_{k_1\leftrightarrow -k'} && \text{(crossing).} \end{aligned} \tag{23}$$

Because of these relations, only one independent nonvanishing helicity amplitude is left, for which we take

$$|\mathcal{M}_\gamma^{+,-,-,+,+}|^2 = 4Q_f^6 e^6\,\frac{(p\cdot k_1)^2(p\cdot\bar{p})}{(p\cdot k_2)(p\cdot k')(\bar{p}\cdot k_2)(\bar{p}\cdot k')} \tag{24}$$

in agreement with [5]. From this particular $|\mathcal{M}_\gamma|^2$ we can read off all different kinds of singularities that can occur for $\gamma\gamma \to f\bar{f}\gamma$. Firstly, there are collinear poles if f or $\bar{f}$

are scattered into forward or backward directions, similar to forward or backward scattering in $\gamma\gamma \to f\bar{f}$. In this case, we again apply angular cuts, in order to exclude the possibility that f or $\bar{f}$ escape into the beam pipe, i.e., we assume

$$\theta_{\mathrm{cut}} < \theta_f, \theta_{\bar{f}} < 180^\circ - \theta_{\mathrm{cut}}. \tag{25}$$

Secondly, we encounter the usual soft and collinear singularities if k' becomes soft or collinear to p or $\bar{p}$. These singularities are the counterparts to the IR and mass singularities in the virtual QED corrections given in Sect. 3.3.1; they have to be regularized, as in the virtual case, by the infinitesimal photon mass λ and the fermion mass m_f. In the following, we describe three different procedures for the treatment of these singularities.

(i) IR phase-space slicing and effective collinear factors. In order to apply phase-space slicing to the IR singularity, we exclude the region $E' < \Delta E$ from the phase space so that the IR singularity is regularized by the cut energy $\Delta E \ll E$. In the soft-photon region $\lambda < E' < \Delta E$, the asymptotic form of the exact differential cross section is known to factorize into the lowest-order cross section without photon emission and a universal eikonal factor, which depends on the photon momentum (see, e.g., [10]). The integration over the soft-photon phase space, which is carried out in the CMS, yields the simple correction factor δ_{soft} to the differential Born cross section $\mathrm{d}\sigma_{\mathrm{Born}}$ for $\gamma\gamma \to f\bar{f}$:

$$\delta_{\mathrm{soft}} = -Q_f^2 \frac{\alpha}{\pi} \left\{ 2 \ln\left(\frac{2\Delta E}{\lambda}\right) \left[1 + \ln\left(\frac{m_f^2}{s}\right)\right] + \frac{1}{2} \ln^2\left(\frac{m_f^2}{s}\right) + \ln\left(\frac{m_f^2}{s}\right) + \frac{\pi^2}{3} \right\}. \tag{26}$$

The factor δ_{soft} does not depend on the polarizations of the produced fermions and of the incoming photons, and its dependence on λ obviously cancels against the one in $\delta_{\mathrm{QED}}^{\mathrm{virt}}$ given in Sect. 3.3.1.

The remaining phase-space integration in (21) with $E' > \Delta E$ still contains the collinear singularities in the regions in which $(p \cdot k')$ or $(\bar{p} \cdot k')$ is small. In these regions, however, the asymptotic behaviour of the differential cross section (including its dependence on m_f) has a well-known form (see, e.g., [16]). The singular terms are universal and factorize from $\mathrm{d}\sigma_{\mathrm{Born}}$. A simple approach to include the collinear regions consists in a suitable modification of $|\mathcal{M}_\gamma|^2$, which was calculated for $m_f = 0$. More precisely, $|\mathcal{M}_\gamma|^2$ is multiplied by an *effective collinear factor* that is equal to 1 up to terms of $\mathcal{O}(m_f^2/s)$ outside the collinear regions, but replaces the poles in $(p \cdot k')$ and $(\bar{p} \cdot k')$ by the correctly mass-regularized behaviour. Explicitly, the described substitution reads

$$\sum_{\lambda'=\pm1} |\mathcal{M}_\gamma^{\lambda_1,\lambda_2,\sigma,\bar{\sigma},\lambda'}|^2 \to \sum_{\tau,\bar{\tau}=\pm1} f_\tau(x_f, E_f, \alpha_f) f_{\bar{\tau}}(x_{\bar{f}}, E_{\bar{f}}, \alpha_{\bar{f}}) \times \sum_{\lambda'=\pm1} |\mathcal{M}_\gamma^{\lambda_1,\lambda_2,\tau\sigma,\bar{\tau}\bar{\sigma},\lambda'}|^2. \tag{27}$$

The functions $f_\pm$ describe collinear photon emission with and without spin flip of the radiating fermion,

$$f_+(x_f, E_f, \alpha_f) = \left(\frac{4E_f^2 \sin^2(\frac{\alpha_f}{2})}{4E_f^2 \sin^2(\frac{\alpha_f}{2}) + m_f^2} \right)^2,$$
$$f_-(x_f, E_f, \alpha_f) = \frac{x_f^2}{x_f^2 + 2x_f + 2} \frac{4m_f^2 E_f^2 \sin^2(\frac{\alpha_f}{2})}{[4E_f^2 \sin^2(\frac{\alpha_f}{2}) + m_f^2]^2},$$
$$x_f = \frac{E'}{E_f}, \tag{28}$$

where $\alpha_f = \angle(\mathbf{k}_f, \mathbf{k}')$ is the angle of the photon emission from f. The functions $f_\pm$ describing photon emission from $\bar{f}$ follow by substituting $f \to \bar{f}$ everywhere. More details on this method can be found in [7,17], where it is applied to $\mathrm{e}^-\gamma \to \mathrm{e}^-\gamma\gamma, \mathrm{e}^-\mathrm{Z}\gamma$.

(ii) IR and collinear phase-space slicing. Instead of using effective collinear factors, one can also apply phase-space slicing to the collinear singularities, i.e., the collinear regions are excluded by the angular cuts $\Delta\alpha < \alpha_f, \alpha_{\bar{f}}$ with $\Delta\alpha \ll 1$. The integration over the collinear regions is particularly simple for final-state radiation (see also [7,17]), since collinear photon emission does not affect the kinematics in the factorized Born cross section $\mathrm{d}\sigma_{\mathrm{Born}}$ of the nonradiative process $\gamma\gamma \to f\bar{f}$. The corrections from collinear photon emission can thus be described by correction factors $\delta_{\mathrm{coll}}^{\pm}$ to $\mathrm{d}\sigma_{\mathrm{Born}}$,

$$\mathrm{d}\sigma_{\mathrm{coll}}(\sigma,\bar{\sigma}) = 2\delta_{\mathrm{coll}}^+ \mathrm{d}\sigma_{\mathrm{Born}}(\sigma,\bar{\sigma}) + \delta_{\mathrm{coll}}^- \mathrm{d}\sigma_{\mathrm{Born}}(-\sigma,\bar{\sigma}) + \delta_{\mathrm{coll}}^- \mathrm{d}\sigma_{\mathrm{Born}}(\sigma,-\bar{\sigma}), \tag{29}$$

where

$$\delta_{\mathrm{coll}}^+ = Q_f^2 \frac{\alpha}{2\pi} \left\{ \left[\ln\left(\frac{m_f^2}{\Delta\alpha^2 E^2}\right) + 1 \right] \times \left[2\ln\left(\frac{\Delta E}{E}\right) + \frac{3}{2} \right] + \frac{5}{2} - \frac{2\pi^2}{3} \right\},$$
$$\delta_{\mathrm{coll}}^- = Q_f^2 \frac{\alpha}{4\pi}. \tag{30}$$

Note that the sum of the soft and collinear corrections without spin flip, i.e., $\delta_{\mathrm{soft}} + 2\delta_{\mathrm{coll}}^+$, comprises all IR- and mass-singular terms originating from real-photon emission; after adding $\delta_{\mathrm{QED}}^{\mathrm{virt}}$, all $\ln\lambda$ and $\ln m_f$ terms drop out. On the other hand, the corrections due to δ_{coll}^- are the only sources for final-state $f\bar{f}$ pairs with $\sigma = \bar{\sigma}$.

(iii) Subtraction method. The idea of the subtraction method is to subtract and to add a simple auxiliary function from the singular integrand. This auxiliary function has to be chosen such that it cancels all singularities of

the original integrand so that the phase-space integration of the difference can be performed numerically. Moreover, the auxiliary function has to be simple enough so that it can be integrated over the singular regions analytically, when the subtracted contribution is added again. In the following, we apply a modification of the so-called "dipole formalism" [18], which was formulated for next-to-leading-order QCD corrections involving unpolarized massless partons. In the modified version of this formalism, all divergences are regularized by photon and fermion masses, and polarization is allowed [19].

When the dipole formalism is applied to photon radiation, the combinatorial part in the construction of the subtraction function is rather simple. The subtraction function consists of contributions labelled by all ordered pairs of charged external particles, one of which is called *emitter*, the other *spectator*. Specifically, for $\gamma\gamma \to f\bar{f}\gamma$ we get two contributions: In the first case, f plays the role of the emitter and $\bar{f}$ the one of the spectator, and in the second case, the roles are reversed. The two functions that are subtracted from $\sum_{\lambda'} |\mathcal{M}_\gamma|^2$ in the phase-space integral are given explicitly by

$$\begin{aligned}
|\mathcal{M}_{\text{sub},1}^{\lambda_1,\lambda_2,\sigma,\bar{\sigma}}|^2 &= \frac{Q_f^2 e^2}{(p\cdot k')}\left[\frac{2}{1-z_1(1-y_1)} - 1 - z_1\right] \\
&\quad \times |\mathcal{M}_{\text{Born}}^{\lambda_1,\lambda_2,\sigma,\bar{\sigma}}(s,t_1,u_1)|^2, \\
|\mathcal{M}_{\text{sub},2}^{\lambda_1,\lambda_2,\sigma,\bar{\sigma}}|^2 &= \frac{Q_f^2 e^2}{(\bar{p}\cdot k')}\left[\frac{2}{1-z_2(1-y_2)} - 1 - z_2\right] \\
&\quad \times |\mathcal{M}_{\text{Born}}^{\lambda_1,\lambda_2,\sigma,\bar{\sigma}}(s,t_2,u_2)|^2,
\end{aligned} \tag{31}$$

where $|\mathcal{M}_{\text{Born}}^{\lambda_1\lambda_2\sigma\bar{\sigma}}|^2$ are the squared Born helicity amplitudes (7) for $\gamma\gamma \to f\bar{f}$. The auxiliary variables y_i and z_i $(i = 1, 2)$ are defined by

$$\begin{aligned}
&y_1 = \frac{pk'}{p\bar{p} + pk' + \bar{p}k'} = \frac{2pk'}{s}, \quad z_1 = \frac{p\bar{p}}{p\bar{p} + \bar{p}k'}, \\
&y_2 = y_1\Big|_{p\leftrightarrow\bar{p}}, \quad z_2 = z_1\Big|_{p\leftrightarrow\bar{p}},
\end{aligned} \tag{32}$$

and the Mandelstam variables t_i and u_i are defined as in (3), but for auxiliary momenta p_i and $\bar{p}_i$,

$$\begin{aligned}
t_i &= (k_1 - p_i)^2 = (k_2 - \bar{p}_i)^2 = -4E^2 \sin^2\tfrac{\theta_i}{2}, \\
u_i &= (k_1 - \bar{p}_i)^2 = (k_2 - p_i)^2 = -4E^2 \cos^2\tfrac{\theta_i}{2}.
\end{aligned} \tag{33}$$

The auxiliary momenta are chosen such that $p_i \to p$ and $\bar{p}_i \to \bar{p}$ in the IR limit $k' \to 0$, that $p_1 \to p + k'$ and $\bar{p}_1 \to \bar{p}$ if k becomes collinear to p, and that $\bar{p}_2 \to \bar{p} + k'$ and $p_2 \to p$ if k becomes collinear to $\bar{p}$. Moreover, the auxiliary momenta obey momentum conservation, $p + \bar{p} + k' = p_i + \bar{p}_i$, and the mass-shell conditions, $p_i^2 = \bar{p}_i^2 = 0$,

$$\begin{aligned}
p_1 &= p + k' - \frac{y_1}{1-y_1}\bar{p}, \quad & \bar{p}_1 &= \frac{1}{1-y_1}\bar{p}, \\
p_2 &= \frac{1}{1-y_2}p, & \bar{p}_2 &= \bar{p} + k' - \frac{y_2}{1-y_2}p.
\end{aligned} \tag{34}$$

From this definition we can also deduce that the scattering angles θ_i, which are defined in (33), are given by $\theta_1 = \theta_{\bar{f}}$ and $\theta_2 = \theta_f$.

Checking that $\sum_i |\mathcal{M}_{\text{sub},i}|^2$ has the same asymptotic structure as $\sum_{\lambda'} |\mathcal{M}_\gamma|^2$ in the soft limit $k' \to 0$ and in the collinear limits $(p\cdot k'), (\bar{p}\cdot k') \to 0$ is straightforward; consequently the phase-space integral

$$\begin{aligned}
\sigma_1 &= \frac{N_f^{\text{c}}}{2s}\int \mathrm{d}\Gamma \left[\left(\sum_{\lambda'} |\mathcal{M}_\gamma|^2\right) g_{\text{cut}}(\theta_f) g_{\text{cut}}(\theta_{\bar{f}})\right. \\
&\quad \left. - \left(\sum_i |\mathcal{M}_{\text{sub},i}|^2 g_{\text{cut}}(\theta_i)\right)\right] \\
&= \frac{N_f^{\text{c}}}{2s}\int \mathrm{d}\Gamma \left[\left(\sum_{\lambda'} |\mathcal{M}_\gamma|^2\right) g_{\text{cut}}(\theta_f) g_{\text{cut}}(\theta_{\bar{f}})\right. \\
&\quad \left. - \left(|\mathcal{M}_{\text{sub},1}|^2 g_{\text{cut}}(\theta_{\bar{f}})\right) - \left(|\mathcal{M}_{\text{sub},2}|^2 g_{\text{cut}}(\theta_f)\right)\right]
\end{aligned} \tag{35}$$

is finite and can be performed numerically. In (35) we indicate the phase-space cuts from (25) explicitly by the step functions (9). In the subtracted part, the cuts are applied to the auxiliary momenta p_i, $\bar{p}_i$. Since these approach the physical momenta of the final-state fermions in the singular regions, the cuts do not obstruct the cancellation of the singularities in (35) as long as they avoid the singularities. The last equality holds because $\theta_2 = \theta_f$ and $\theta_1 = \theta_{\bar{f}}$ in our case.

For the full cross section we have to add the integral of $\sum_i |\mathcal{M}_{\text{sub},i}|^2$ that is evaluated with the regulators λ and m_f [19]. The functions $|\mathcal{M}_{\text{sub},i}|^2$ are constructed such that the integration over the photon phase space can be performed analytically, leading to universal correction factors $\delta_{\text{sub}}^{\pm}$ on the Born cross section σ_{Born} (10) for $\gamma\gamma \to f\bar{f}$,

$$\begin{aligned}
\sigma_2(\sigma,\bar{\sigma}) &= 2\delta_{\text{sub}}^{+}\sigma_{\text{Born}}(\sigma,\bar{\sigma}) + \delta_{\text{sub}}^{-}\sigma_{\text{Born}}(-\sigma,\bar{\sigma}) \\
&\quad + \delta_{\text{sub}}^{-}\sigma_{\text{Born}}(\sigma,-\bar{\sigma}),
\end{aligned} \tag{36}$$

where

$$\begin{aligned}
\delta_{\text{sub}}^{+} &= Q_f^2 \frac{\alpha}{2\pi}\left\{\ln\left(\frac{\lambda^2}{s}\right)\ln\left(\frac{m_f^2}{s}\right) + \ln\left(\frac{\lambda^2}{s}\right)\right. \\
&\quad \left. - \frac{1}{2}\ln^2\left(\frac{m_f^2}{s}\right) + \frac{1}{2}\ln\left(\frac{m_f^2}{s}\right) + \frac{5}{2} - \frac{2\pi^2}{3}\right\}, \\
\delta_{\text{sub}}^{-} &= Q_f^2 \frac{\alpha}{4\pi}.
\end{aligned} \tag{37}$$

In (36), the Born cross sections σ_{Born} are evaluated with the restriction (8) on the scattering angle θ: $\theta_{\text{cut}} < \theta < 180^\circ - \theta_{\text{cut}}$. As required, the IR- and mass-singular terms in $2\delta_{\text{sub}}^{+}$ exactly cancel against those terms in $\delta_{\text{QED}}^{\text{virt}}$. The final result for the real-photon contribution to the cross section is given by $\sigma_\gamma = \sigma_1 + \sigma_2$.

4 Numerical results

For the numerical evaluation, we have adopted the parameters [20]

$$\begin{aligned}
&\alpha = 1/137.0359895, \\
&M_{\text{W}} = 80.41\,\text{GeV}, \\
&M_{\text{Z}} = 91.187\,\text{GeV}.
\end{aligned} \tag{38}$$

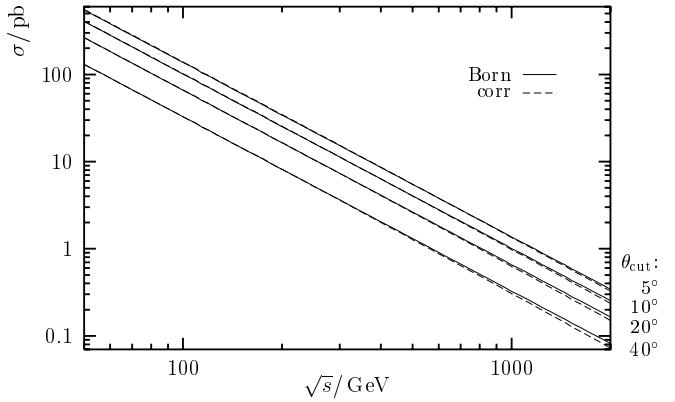

Fig. 5. Lowest-order and $\mathcal{O}(\alpha)$-corrected cross section for $\gamma\gamma \to \mathrm{e}^-\mathrm{e}^+$

We need not specify the masses m_f of the light fermions, since these are only kept as regulating parameters, and drop out in all considered observables. We discuss only unpolarized cross sections. The nonvanishing cross sections for polarized initial states and unpolarized final states differ from the unpolarized cross sections only by the normalization.

In Fig. 5, we show the lowest-order and the $\mathcal{O}(\alpha)$-corrected cross sections for $\gamma\gamma \to \mathrm{e}^-\mathrm{e}^+$ for the angular cuts $\theta_{\mathrm{cut}} = 5°, 10°, 20°, 40°$. The Born cross sections vary from 137 pb to 33 pb for these cuts at $\sqrt{s} = 100\,\mathrm{GeV}$; they scale like $1/s$ if the cut angle θ_{cut} is chosen to be energy-independent, as can be seen in (10). Since the impact of the $\mathcal{O}(\alpha)$ corrections is hardly visible in Fig. 5, we show the relative QED and weak corrections to $\gamma\gamma \to \mathrm{e}^-\mathrm{e}^+$ separately in Fig. 6 for two angular cuts.

For an energy-independent angular cut θ_{cut}, the QED corrections (see Fig. 6) do not depend on the scattering energy for $s \gg m_{\mathrm{e}}^2$, since all electron-mass singularities cancel, and s is the only scale that survives. The cancellation of all potentially large QED corrections such as $\alpha \ln(m_{\mathrm{e}}^2/s)/\pi$ implies that the resulting QED correction is of the order of $\mathcal{O}(\alpha/\pi)$, i.e., of the order of several per mille. The numerical results confirm this expectation. The weak corrections stay below 0.05% for energies below 100 GeV, and tend to zero in the low-energy limit. In other words, weak-boson exchange decouples below the electroweak scale. Above 100 GeV, the weak corrections become sizeable and develop a peak at $\sqrt{s} = 2M_{\mathrm{W}}$, originating from diagrams with a W-pair cut in the s channel. For energies up to 1 TeV, δ_{weak} reaches a negative percentage, then becomes more and more negative with increasing energy, crossing the -10% mark at about 2 TeV. The large negative corrections at high energies are due to Sudakov-type logarithms, such as $\alpha \ln^2(M_{\mathrm{W}}^2/s)/\pi$, and the dominant contributions stem from W-boson exchange.

The lowest-order cross sections and the relative QED corrections for $\gamma\gamma \to f\bar{f}$ with arbitrary fermion flavour can be easily obtained from the results on $\gamma\gamma \to \mathrm{e}^-\mathrm{e}^+$ by multiplying the results for the $\mathrm{e}^-\mathrm{e}^+$ pair by the factors $N_f^{\mathrm{c}} Q_f^4$ and Q_f^2, respectively. In particular, this means that the QED corrections to nonleptonic channels become even

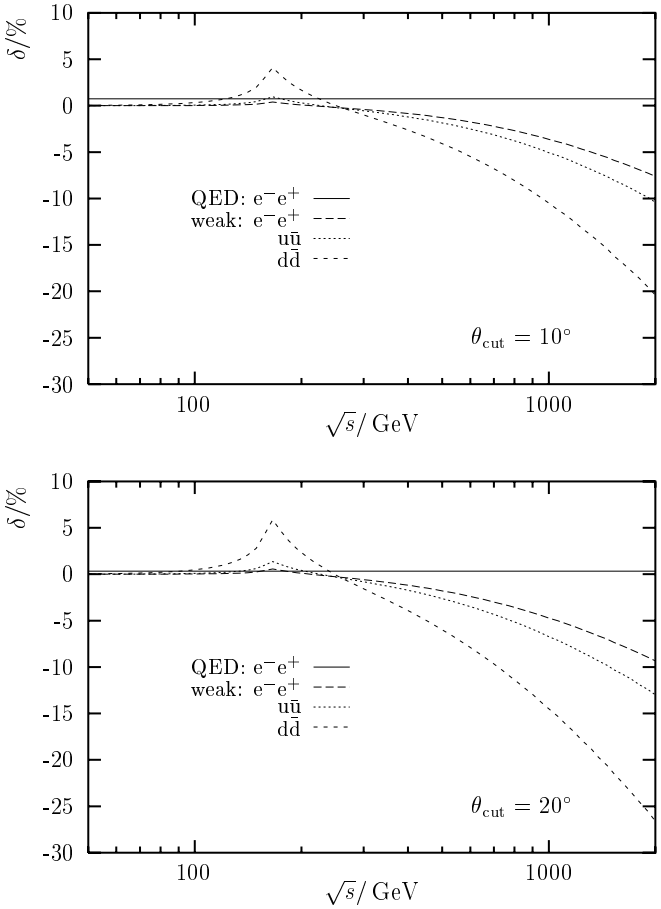

Fig. 6. Relative QED and weak corrections to $\gamma\gamma \to \mathrm{e}^-\mathrm{e}^+$, and weak corrections to $\gamma\gamma \to \mathrm{u}\bar{\mathrm{u}}, \mathrm{d}\bar{\mathrm{d}}$

smaller. The weak corrections, however, depend on the fermion flavour in a nontrivial way. Therefore, the relative weak corrections are explicitly shown also for up-type and down-type light quarks in Fig. 6. The shape of the weak corrections to light-quark-pair production is qualitatively similar to the one for lepton-pair production, but the light-quark-pair-production weak corrections are larger in size. For high energies we roughly get $\delta_{\mathrm{weak}}^{\mathrm{u}\bar{\mathrm{u}}}/\delta_{\mathrm{QED}}^{\mathrm{e}^-\mathrm{e}^+} \sim 1.4$ and $\delta_{\mathrm{weak}}^{\mathrm{d}\bar{\mathrm{d}}}/\delta_{\mathrm{QED}}^{\mathrm{e}^-\mathrm{e}^+} \sim 3$. This enhancement of the relative weak corrections is mainly due to the suppression of the lowest-order cross section by the quark charges, which is not present in the dominating CC corrections.

Table 1 summarizes the discussed results by providing some representative numbers. At high energies, the weak corrections are dominated by the CC corrections. The NC corrections are at the level of 1% at 2 TeV.

We conclude our numerical discussion by a short comparison of the different methods for the singular phase-space integration for real-photon emission, which are described in Sect. 3.3.2. Table 2 compares numerical results on δ_{QED} that have been obtained by performing the multidimensional integration with Vegas [21], using the same Vegas parameters for each integration. The subtraction method leads to an integration error that is smaller by a factor of 10–20 with respect to the results from the two

Table 1. Integrated Born cross section for $\gamma\gamma \to e^-e^+$, the corresponding relative QED and weak corrections, and the weak corrections to $\gamma\gamma \to u\bar{u}, d\bar{d}$

$\sqrt{s}$/ GeV	θ_{cut}	$\sigma_{\mathrm{Born}}^{e^-e^+}$ / pb	$\delta_{\mathrm{QED}}^{e^-e^+}$ /%	$\delta_{\mathrm{weak}}^{e^-e^+}$ /%	$\delta_{\mathrm{weak}}^{u\bar{u}}$/%	$\delta_{\mathrm{weak}}^{d\bar{d}}$/%
10	5°	13722	1.30	0.00	0.00	0.00
	10°	10130	0.74	0.00	0.00	0.00
	20°	6595.2	0.33	0.00	0.00	0.00
	40°	3270.9	−0.02	0.00	0.00	0.00
100	5°	137.22	1.30	0.02	0.05	0.26
	10°	101.30	0.74	0.02	0.07	0.34
	20°	65.952	0.33	0.03	0.10	0.49
	40°	32.709	−0.02	0.05	0.14	0.73
500	5°	5.4889	1.30	−0.97	−1.39	−3.03
	10°	4.0520	0.74	−1.29	−1.85	−4.08
	20°	2.6381	0.33	−1.78	−2.62	−5.97
	40°	1.3084	−0.02	−2.47	−3.79	−9.23
1000	5°	1.3722	1.30	−2.81	−3.88	−7.95
	10°	1.0130	0.74	−3.61	−5.03	−10.49
	20°	0.65952	0.33	−4.70	−6.69	−14.48
	40°	0.32709	−0.02	−5.95	−8.78	−20.11
2000	5°	0.34306	1.30	−6.18	−8.27	−15.92
	10°	0.25325	0.74	−7.62	−10.35	−20.38
	20°	0.16488	0.33	−9.33	−12.98	−26.60
	40°	0.081773	−0.02	−11.15	−15.98	−34.55

Table 2. Comparison of results for the QED correction δ_{QED}/% at $\sqrt{s} = 500\,\mathrm{GeV}$, obtained by the different methods for bremsstrahlung corrections described in Sect. 3.3

Method	$\Delta E/E$	$\Delta\alpha$/rad	$\theta_{\mathrm{cut}} = 10°$	$\theta_{\mathrm{cut}} = 20°$
IR slicing and	10^{-3}	–	0.798 ± 0.016	0.345 ± 0.014
effective collinear factor	10^{-5}		0.819 ± 0.029	0.329 ± 0.024
IR and collinear slicing	10^{-3}	10^{-3}	0.756 ± 0.011	0.3302 ± 0.0083
		10^{-5}	0.784 ± 0.015	0.349 ± 0.013
	10^{-5}	10^{-3}	0.734 ± 0.019	0.323 ± 0.015
		10^{-5}	0.808 ± 0.027	0.324 ± 0.022
Subtraction scheme	–	–	0.74447 ± 0.00080	0.33124 ± 0.00069

versions of phase-space slicing. While there are still large compensations between the phase-space integral and the (semi-)analytically calculated singular parts in the slicing approach, for the subtraction method all compensations take place between $\delta_{\mathrm{QED}}^{\mathrm{virt}}$ and $2\delta_{\mathrm{sub}}^{+}$, which are computed without delicate numerical integrations. Table 2 illustrates the consistent application of the different methods, but the numbers for the smaller cut $\theta_{\mathrm{cut}} = 10°$ also reveal that Monte Carlo integration by Vegas tends to underestimate integration errors if the integrand becomes complicated, although it has been smoothed by appropriate transformations of the integration variables[4]. The subtraction method is distinguished by the fact that it is less sensitive to numerical uncertainties.

[4] Repeated evaluations for $\theta_{\mathrm{cut}} = 10°$ show that the results obtained with the two slicing variants come closer and closer to that of the subtraction method given in Table 2 if the statistics is improved.

5 Summary

The $\mathcal{O}(\alpha)$ corrections to $\gamma\gamma \to f\bar{f}$ in the standard model have been calculated for arbitrary light fermions f, i.e., fermion-mass effects are neglected. Compact analytical results for the cross sections have been listed for arbitrary polarization configurations, rendering their incorporation in computer codes very simple. Numerical results on the corrections to integrated cross sections have been discussed.

The corrections are classified into QED and purely weak corrections. Owing to the cancellation of all mass-singular contributions between virtual and real-photon corrections, the QED corrections to integrated cross sections are of $\mathcal{O}(Q_f^2\alpha/\pi)$ for all energies, i.e., of the order of some per mille. For lepton-pair production, the weak corrections are negligible below the weak-boson scale, reach a moderate negative percentage at 1 TeV, and reduce the cross section more and more with increasing energy, crossing -10% at about 2 TeV. For up- and down-type quarks, the weak corrections to the integrated cross sections show the same qualitative features as in the leptonic case, but the corrections are a few times larger. The weak corrections vanish whenever the differential cross sections develop t- or u-channel poles, i.e., the relative corrections can be enhanced or suppressed by appropriate angular cuts.

The smallness and the structure of the corrections to $\gamma\gamma \to \mathrm{e}^-\mathrm{e}^+, \mu^-\mu^+$ underline the suitability of these processes as a luminosity monitor. In particular, the corrections do not exhibit large uncertainties induced by hadronic effects in the photonic vacuum polarization or by the less-precisely-known top quark, or even by the unknown Higgs-boson mass. The results for the processes $\gamma\gamma \to q\bar{q}$ provide a valuable input for QCD studies.

Appendix

List of scalar integrals

Here we list all scalar one-loop integrals that are needed for the evaluation of the virtual corrections given in Sect. 3. We use the same definition of the momentum-space integrals and of the arguments of the standard functions B_0, C_0, and D_0 as given in the appendix of [7]. The relevant integrals are calculated for the limit $|s|, |t|, |u|, M_\mathrm{W}^2 \gg m_f^2, m_{f'}^2$. By definition, Mandelstam variables with a hat get an infinitesimal imaginary part $\mathrm{i}\epsilon$, with $\epsilon > 0$, i.e., $\hat{s} = s + \mathrm{i}\epsilon$, etc. After supplying this imaginary part where necessary, all scalar integrals can also be obtained from those for Compton scattering in [7], with the use of crossing symmetry. Scalar functions that are related by the interchange of t and u are given generically, with the abbreviation $r = t, u$.

All needed 2-point functions B_0 are calculated in D space-time dimensions with $D \to 4$. Instead of using B_0 directly, we have preferred to introduce the UV-finite combinations

$$
\begin{aligned}
&B_0(s,0,0) - B_0(0,0,M_\mathrm{W}) = B(s) \\
&\quad = \ln\left(-\frac{M_\mathrm{W}^2}{\hat{s}}\right) + 1, \\
&B_0(r,0,M_\mathrm{W}) - B_0(0,0,M_\mathrm{W}) = B_\mathrm{w}(r) \\
&\quad = \left(\frac{M_\mathrm{W}^2}{r} - 1\right)\ln\left(1 - \frac{\hat{r}}{M_\mathrm{W}^2}\right) + 1, \\
&B_0(s,M_\mathrm{W},M_\mathrm{W}) - B_0(0,0,M_\mathrm{W}) = B_\mathrm{ww}(s) \\
&\quad = \beta_\mathrm{w}\ln(x_\mathrm{w}) + 1,
\end{aligned}
\tag{A.1}
$$

with the abbreviations

$$
x_\mathrm{w} = \frac{\beta_\mathrm{w} - 1}{\beta_\mathrm{w} + 1}, \qquad \beta_\mathrm{w} = \sqrt{1 - \frac{4M_\mathrm{W}^2}{\hat{s}}}. \tag{A.2}
$$

The relevant 3- and 4-point functions are given by

$$
\begin{aligned}
&C_0(0,0,s,m_{f'},m_{f'},m_{f'}) = C(s) = \frac{1}{2s}\ln^2\left(-\frac{\hat{s}}{m_{f'}^2}\right), \\
&C_0(m_f^2,0,r,M_\mathrm{W},m_{f'},m_{f'}) = \bar{C}_\mathrm{w}(r) \\
&\quad = \frac{1}{r}\left[\mathrm{Li}_2\left(\frac{r}{M_\mathrm{W}^2}\right) - \ln\left(\frac{m_{f'}^2}{M_\mathrm{W}^2 - r}\right)\ln\left(1 - \frac{r}{M_\mathrm{W}^2}\right)\right], \\
&C_0(0,0,s,0,M_\mathrm{W},0) = C_\mathrm{w}(s) \\
&\quad = \frac{1}{s}\left[-\mathrm{Li}_2\left(1 + \frac{\hat{s}}{M_\mathrm{W}^2}\right) + \frac{\pi^2}{6}\right], \\
&C_0(0,0,r,0,M_\mathrm{W},M_\mathrm{W}) = \bar{C}_\mathrm{ww}(r) = -\frac{1}{r}\mathrm{Li}_2\left(\frac{r}{M_\mathrm{W}^2}\right), \\
&C_0(0,0,s,M_\mathrm{W},0,M_\mathrm{W}) = C_\mathrm{ww}(s) = \frac{1}{s}\ln^2(x_\mathrm{w}), \\
&C_0(0,0,s,M_\mathrm{W},M_\mathrm{W},M_\mathrm{W}) = C_\mathrm{www}(s) = \frac{1}{2s}\ln^2(x_\mathrm{w}),
\end{aligned}
\tag{A.3}
$$

$$
\begin{aligned}
&D_0(0,0,0,0,s,r,m_{f'},M_\mathrm{W},m_{f'},m_{f'}) = D_\mathrm{w}(s,r) \\
&\quad = \frac{1}{s(r - M_\mathrm{W}^2)}\left[\mathrm{Li}_2\left(1 + \frac{\hat{s}}{M_\mathrm{W}^2}\right)\right. \\
&\qquad -4\,\mathrm{Li}_2\left(\frac{r}{r - M_\mathrm{W}^2}\right) + \frac{1}{2}\ln^2\left(-\frac{\hat{s}}{m_{f'}^2}\right) \\
&\qquad \left.+2\ln\left(-\frac{\hat{s}}{m_{f'}^2}\right)\ln\left(1 - \frac{r}{M_\mathrm{W}^2}\right) - \frac{\pi^2}{6}\right], \\
&D_0(0,0,0,0,t,u,M_\mathrm{W},M_\mathrm{W},m_{f'},m_{f'}) = D_\mathrm{ww}(t,u) \\
&\quad = \frac{1}{tu - M_\mathrm{W}^2(u+t)} \\
&\qquad \times\left[2\,\mathrm{Li}_2\left(1 + x_{tu} - \frac{\hat{t}}{M_\mathrm{W}^2}x_{tu}\right)\right. \\
&\qquad +2\eta\left(-x_{tu}, 1 - \frac{\hat{t}}{M_\mathrm{W}^2}\right)\ln\left(1 + x_{tu} - \frac{\hat{t}}{M_\mathrm{W}^2}x_{tu}\right) \\
&\qquad \left.-2\,\mathrm{Li}_2(1 + x_{tu}) + \ln\left(\frac{M_\mathrm{W}^2 - t}{m_{f'}^2}\right)\ln\left(1 - \frac{t}{M_\mathrm{W}^2}\right)\right]
\end{aligned}
$$

$$+ (t \leftrightarrow u),$$

$$\text{with} \quad x_{tu} = \frac{M_{\mathrm{W}}^2(\hat{t}+\hat{u})}{\hat{t}\hat{u} - M_{\mathrm{W}}^2(\hat{t}+\hat{u})},$$

$$\begin{aligned} D_0(0,0,0,0,s,r,M_{\mathrm{W}},0,M_{\mathrm{W}},M_{\mathrm{W}}) &= D_{\mathrm{www}}(s,r) \\ &= \frac{1}{\sqrt{\hat{s}^2(\hat{r}-M_{\mathrm{W}}^2)^2 - 4\hat{r}^2\hat{s}M_{\mathrm{W}}^2}} \sum_{n=1}^{2} (-1)^{n+1} \\ &\quad \times \Bigg[3\,\mathrm{Li}_2(1+x_n) - \mathrm{Li}_2\left(1 + \frac{x_n M_{\mathrm{W}}^2}{M_{\mathrm{W}}^2 - \hat{r}}\right) \\ &\quad -\eta\left(-x_n, \frac{M_{\mathrm{W}}^2}{M_{\mathrm{W}}^2-\hat{r}}\right) \ln\left(1 + \frac{x_n M_{\mathrm{W}}^2}{M_{\mathrm{W}}^2-\hat{r}}\right) \\ &\quad + \ln\left(1 - \frac{\hat{r}}{M_{\mathrm{W}}^2}\right) \ln(-x_n) - \sum_{\tau=\pm 1} \Big\{ \mathrm{Li}_2\left(1 + x_n x_{\mathrm{w}}^{\tau}\right) \\ &\quad + \eta\left(-x_n, x_{\mathrm{w}}^{\tau}\right) \ln\left(1 + x_n x_{\mathrm{w}}^{\tau}\right) \Big\} \Bigg], \end{aligned} \tag{A.4}$$

with x_{w} and β_{w} as given in (A.2), and

$$x_{1,2} = \frac{\hat{s}(\hat{r}-M_{\mathrm{W}}^2) - 2\hat{r}M_{\mathrm{W}}^2 \pm \sqrt{\hat{s}^2(\hat{r}-M_{\mathrm{W}}^2)^2 - 4\hat{r}^2\hat{s}M_{\mathrm{W}}^2}}{2(\hat{r}+\hat{s})M_{\mathrm{W}}^2}. \tag{A.5}$$

The dilogarithm $\mathrm{Li}_2(x)$ and the function $\eta(x,y)$ are defined as usual:

$$\mathrm{Li}_2(x) = -\int_0^x \frac{\mathrm{d}t}{t}\, \ln(1-t), \quad -\pi < \arg(1-x) < \pi, \tag{A.6}$$

$$\eta(x,y) = \ln(xy) - \ln(x) - \ln(y), \quad -\pi < \arg(x), \arg(y) < \pi. \tag{A.7}$$

References

1. I.F. Ginzburg, G.L. Kotkin, V.G. Serbo and V.I. Telnov, Nucl. Instr. Meth. **205**, 47 (1983); I.F. Ginzburg, G.L. Kotkin, S.L. Panfil, V.G. Serbo and V.I. Telnov, Nucl. Instr. Meth. **219**, 5 (1984)
2. R. Brinkmann et al., Nucl. Instr. Meth. **A406**, 13 (1998)
3. S. Brodsky, P.M. Zerwas, Nucl. Instr. Meth. **A355**, 19 (1995); M. Chanowitz, Nucl. Instr. Meth. **A355**, 42 (1995); I. Ginzburg, Nucl. Instr. Meth. **A355**, 63 (1995)
4. F.A. Berends, R. Gastmans, Nucl. Phys. **B61**, 414 (1973), in Electromagnetic Interactions of Hadrons, Vol. 2, edited by A. Donnachie, G. Shaw (Plenum Press, New York, 1978), p. 471
5. F.A. Berends, P. de Causmaecker, R. Gastmans, R. Kleiss, W. Troost, T.T. Wu, Nucl. Phys. **206**, 61 (1982)
6. M. Böhm, T. Sack, Z. Phys. **C33**, 157 (1986)
7. S. Dittmaier, Nucl. Phys. **B423**, 384 (1994)
8. A. Denner, S. Dittmaier, M. Strobel, Phys. Rev. **D53**, 44 (1995)
9. J. Küblbeck, M. Böhm, A. Denner, Comput. Phys. Commun. **60** (1990) 165; H. Eck, J. Küblbeck, Guide to FeynArts 1.0 (University of Würzburg 1992)
10. A. Denner, Fortschr. Phys. **41** (1993) 307
11. G. Passarino, M. Veltman, Nucl. Phys. **B160**, 151 (1979)
12. G. 't Hooft, M. Veltman, Nucl. Phys. **B153**, 365 (1979); W. Beenakker, A. Denner, Nucl. Phys. **B338**, 349 (1990); A. Denner, U. Nierste, R. Scharf, Nucl. Phys. **B367**, 637 (1991)
13. R. Mertig, M. Böhm, A. Denner, Comput. Phys. Commun. **64** (1991) 345; R. Mertig, Guide to FeynCalc 1.0, (University of Würzburg 1992)
14. S. Wolfram, Mathematica – A System for Doing Mathematics by Computer (Addison-Wesley, Redwood City, CA, 1988)
15. S. Dittmaier, Phys. Rev. **D59**, 016007 (1999)
16. F.A. Berends et al., Nucl. Phys. **B206**, 53 (1982); R. Kleiss, Z. Phys. **C33**, 433 (1987)
17. M. Böhm, S. Dittmaier, Nucl. Phys. **B412**, 39 (1993)
18. S. Catani, M.H. Seymour, Phys. Lett. **B378**, 287 (1996); Nucl. Phys. **B485**, 291 (1997). Erratum, ibid. **B510**, 503 (1997)
19. S. Dittmaier, BI-TP 99/09, hep-ph/9904440; M. Roth, Dissertation, ETH Zurich, in preparation
20. C. Caso et al., Particle Data Group, Eur. Phys. J. **C3**, 1 (1998)
21. G.P. Lepage, J. Comput. Phys. **27**, 192 (1978); Cornell University preprint (1980) [CLNS-80/447]